DOI: 10.1021/ma100175t

Macromolecules
ARTICLE

DNA Collisions with a Large, Conducting Post

Daniel W. Trahan and Patrick S. Doyle*

Department of Chemical Engineering, Massachusetts Institute of Technology, Cambridge, Massachusetts 02139

Received January 25, 2010; Revised Manuscript Received April 23, 2010

ABSTRACT: We theoretically treat the problem of DNA collisions with large, ideally conducting posts during electrophoresis. We exploit a separation of time and length scales that allows the problem to be broken into two connected problems: (i) compression of a molecule against a flat wall by an applied transverse field and (ii) transport of a molecule across the post surface due to both tangential diffusion and convection. We address the former using a combination of statistical mechanics and blob theory and the latter utilizing a Fokker−Planck approach. The theoretical predictions are then compared with the results of Brownian dynamics simulations.

1. Introduction

The development of microfluidics and "lab-on-a-chip" devices has opened a new era for the study of DNA electrophoresis and polymer physics more generally. Such devices have provided platforms to study fundamental problems in polymer physics,[1−6] and along the way, they have found applications in DNA separations[7−9] and genomic mapping.[10,11] In particular, one problem that has received considerable attention is the collision of a DNA molecule with a cylindrical post.[12−18]

Post arrays and similar devices have been used to achieve separation of large DNA molecules.[7,19,20] When a DNA molecule is electrophoretically or hydrodynamically driven into a post, it frequently forms a hook by wrapping around the post and into a hairpin-like configuration.[13,14,16,21−23] The subsequent unhooking process, which is often described by a rope-over-pulley model, results in a length-dependent unhooking time and establishes the basis for length-based separations in large arrays of posts.[12,13,21,22,24]

More fundamentally, collisions offer a simple way to manipulate individual molecules by applying forces on the molecular length scale. For example, post collisions have been used to deform DNA molecules so that their ensuing relaxation processes can be studied.[2,5] In addition, our group has exploited collisions to "precondition" DNA for subsequent stretching in an elongational field[25] to overcome molecular individualism.[26] Cylindrical posts have also been used to create field gradients near the post surface that can stretch and deform molecules.[15,27]

Past post work has tended to focus on the small post limit where the posts are much smaller than the equilibrium DNA coil size. These "point obstacles" virtually guarantee the formation of a large number of molecular hooks as long as the field strength is strong enough[28] and the posts are properly positioned.[29,30] However, from a theoretical perspective, modeling of the direct interactions between a point obstacle, and a molecule is fairly simple with the post being treated as little more than a simple pivot point during a collision.[22] That is not to say that collisions with point obstacles are trivial. The dynamics of such events can be quite complex,[22] but the characteristics of the post itself are completely neglected. When the finite size of the posts is taken into account, the problem becomes much richer. The relative size of the post becomes important,[14,15] and new types of collision processes are possible (e.g., "roll-offs"[14]). In addition, disturbances of the electrophoretic velocity field due to the presence of the post must be considered.[15,27,31]

When finite-sized posts were first examined, the field disturbances due to the post were neglected, and a uniform field was assumed everywhere.[14] Later, when researchers began to account for the field disturbances, the posts were assumed to be electrically insulating so that the field lines avoid and are repelled by the post surface.[15,16,27] Indeed, on the post surface, the field lines are everywhere tangential to the post. The deformation of the field lines leads to field gradients near the post surface that are able to deform molecules both on the front and backside of the posts,[27] and this deformation aids in hook formation.[15] However, a large number of molecules are quickly swept around the post by the nearly tangential field lines close to the surface. These molecules and their trajectories are only weakly affected by the presence of the post.

2. Problem Statement

In this work, we consider the case of an ideally conducting post. By this, we mean a post whose dielectric constant, ε_p, is much greater than that of the surrounding fluid, ε_f (i.e., $\varepsilon_p \gg \varepsilon_f$). Unlike the insulating case, the field lines for a conducting post, which are shown in Figure 1A, are attracted to and focused by the post. This means that the molecules also tend to be attracted to the post and interact very strongly with it. We are interested in understanding the fundamental physics that govern a molecule that is being electrophoretically driven into an ideally conducting post. Because this is the first attempt to study conducting posts, we only consider linear electrophoresis in our analysis and neglect any nonlinear electrokinetic effects, which may be present.

3. Initial Analysis of Problem

3.1. Qualitative Features of a Collision. The electrophoretic velocity field, $\mu\boldsymbol{E}$, surrounding an ideally conducting post is given by

$$\frac{\mu\boldsymbol{E}}{\mu E_\infty} = -\left[1+\left(\frac{r}{R}\right)^{-2}\right]\cos\theta\mathbf{e}_r + \left[1-\left(\frac{r}{R}\right)^{-2}\right]\sin\theta\mathbf{e}_\theta \quad (1)$$

*Corresponding author. E-mail: pdoyle@mit.edu.

 Published on Web 05/26/2010

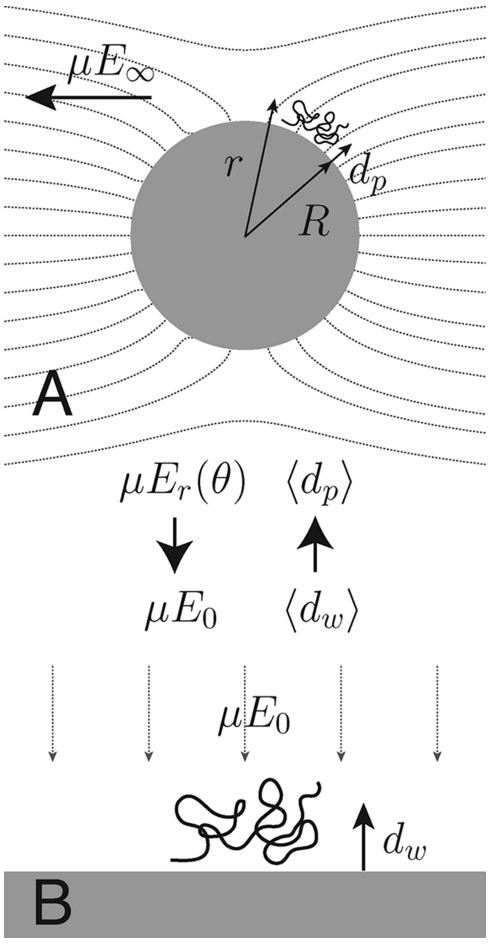

Figure 1. (A) Cartoon of a DNA molecule being electrophoretically driven into an ideally conducting post along with the field lines for the electrophoretic velocity field. This is referred to as the "post problem". (B) DNA molecule is driven into a flat surface by a uniform transverse electrophoretic velocity field. This problem is called the "local problem". Also shown is the information flow between the two problems.

where μ is the electrophoretic mobility of the molecule, E_∞ is the strength of the electric field far away from the post applied in the $-\mathbf{e}_x$ direction, R is the radius of the post, and r and θ give the position in polar coordinates with the origin at the post center.

On the post surface at $r = R$, it is clear from eq 1 that μE_r is strong over most of the surface, whereas μE_θ is identically equal to zero. (See Figure 1A.) Therefore, the field lines always intersect the post surface perpendicularly. On the upstream side of the post ($-\pi/2 < \theta < \pi/2$), the field lines are directed into the post, whereas on the downstream side ($\pi/2 < \theta < 3\pi/2$), the field lines are directed away from and out of the post. As a molecule approaches the post, it is driven into the upstream side of the impenetrable surface. For our study, we have restricted our analysis to large posts, whereby we mean that $R \gg R_g$, where R_g is the radius of gyration of the colliding molecule. This guarantees that hooking of the molecule around the post is precluded and that, for reasonable applied field strengths, the field gradients are weak so that strong stretching of a molecule is also impossible. Therefore, the molecule is compressed and "trapped" against the post by the strong radial field.

There are two mechanisms by which a molecule can "escape" from the post: diffusion and convection. Clearly, the molecule experiences tangential diffusion, and given enough time, diffusion will guarantee eventual escape. But the molecule also experiences a weak tangential velocity, v_θ.

Although $\mu E_\theta = 0$ for $r = R$, for $r > R$, it is nonzero. The strength of μE_θ increases with increasing r, and it is always directed toward the downstream side of the post. Because a compressed molecule still has some finite size, it is exposed to the weak tangential field that exists just off the post surface. This means that the average tangential velocity of the molecule $\langle v_\theta \rangle \neq 0$, and it is slowly convected around the post and finally "escapes". Because $\langle v_\theta \rangle$ depends upon the distance of the molecule from the post surface, we must understand how μE_r compresses the molecule against the post and affects its size.

3.2. Analysis of $\mu \boldsymbol{E}$ Near the Post Surface. Because molecules are "trapped" against the post, we are particularly interested in the behavior of $\mu \boldsymbol{E}$ near the post surface. We can exploit the fact that $R \gg R_g$ and linearize the field around

$$\frac{r}{R} \approx \frac{R + R_g}{R} \approx 1 \tag{2}$$

Additionally, we can replace the radial position, r, with an new coordinate, d_p (Figure 1A), which is the distance from the post surface

$$\frac{d_p}{R} = \frac{r}{R} - 1 \ll 1 \tag{3}$$

Combining these two approximations, we can simplify the nonlinear radial term in eq 1

$$\left(\frac{r}{R}\right)^{-2} \approx 1 - 2\left(\frac{r}{R} - 1\right) \approx 1 - 2\frac{d_p}{R} \tag{4}$$

If we use this result to approximate $\mu \boldsymbol{E}$ near the post surface, then we obtain

$$\frac{\mu \boldsymbol{E}}{\mu E_\infty} \approx -2\cos\theta \mathbf{e}_r + 2\frac{d_p}{R}\sin\theta \mathbf{e}_\theta \tag{5}$$

3.3. Two Connected Problems. The disparity of the length scales due to the large post size, leads to a separation of time scales between the dynamics occurring in each of the dimensions. In the $\mathbf{e}_\theta$ direction, the convective and diffusive time scales are based on the length, R, so the molecular escape time is quite large. Compression in the $\mathbf{e}_r$ direction is due to a competition between convection toward the post surface and diffusion away from it. This results in a time scale for compression based on lengths similar to R_g so that it is very short. Therefore, the dynamics in the $\mathbf{e}_r$ direction occur much more quickly than those in the $\mathbf{e}_\theta$ direction. This allows us to break the collision problem into the two connected problems shown in Figure 1.

We refer to the first of these as the "post problem", which occurs on the scale of the post $\sim R$. From this vantage point, the molecule looks as though it is being transported across the post surface because of a combination of tangential diffusion and convection. The average tangential velocity is approximated based on eq 5

$$\langle v_\theta \rangle \approx 2\mu E_\infty \frac{\langle d_p \rangle}{R}\sin\theta \tag{6}$$

The average distance from the wall $\langle d_p \rangle$ is based on the fast compression dynamics that occur in the radial dimension, and because $\langle d_p \rangle = f(\mu E_r \approx -2\mu E_\infty \cos\theta)$, it varies as the molecule moves across the post surface, but because the

compression dynamics are fast, we can make a pseudosteady approximation and assume that $\langle d_p \rangle$ is always in equilibrium with the local radial field, μE_r.

The second problem shown in Figure 1B is the "local problem" that occurs on the length scale of $\sim R_g$. Effectively, we have "zoomed" in on the molecule. We can neglect the curvature inherent in the post problem because the post surface now looks like a flat wall, and $\mu \boldsymbol{E}$ looks uniform. The only important phenomenon occurring on this scale is the compression of the molecule by the transverse component of the uniform field, which we call μE_0 for the local problem. We can analyze this situation to determine how the average distance from the wall, which we call $\langle d_w \rangle$ for the local problem, depends upon μE_0.

These two problems are clearly connected, as seen in Figure 1. The post problem provides the local problem with the strength of the transverse field ($\mu E_0 = \mu E_r(\theta)$), and in return, the local problem feeds the post problem the average distance from the post ($\langle d_p \rangle = \langle d_w \rangle$) for use in determining the average tangential velocity, $\langle v_\theta \rangle$.

3.4. Approach. In our detailed analysis of the collision problem, we begin by examining the local problem of a Gaussian chain driven into a flat wall by a uniform transverse field. We use a combination of blob theory and statistical mechanics to derive expressions and scalings for $\langle d_w \rangle$ as a function of μE_0. We confirm these scalings using Brownian dynamics simulations.

We then turn to the post problem, where we use our results from the local case to predict $\langle v_\theta \rangle$. After confirming the validity of our predictions using simulations, we incorporate diffusion into our theoretical model by turning to a Fokker–Planck equation and calculating the mean escape time of a molecule based on the initial collision location. These results are compared with simulations as well.

4. Brownian Dynamics Simulation

DNA molecules are modeled as chains of N_b beads connected by $N_s = N_b - 1$ Hookean springs. The equation of motion for the position r_i of the ith bead is

$$\frac{d\boldsymbol{r}_i}{dt} = \mu \boldsymbol{E}(\mathbf{r}_i) + \frac{1}{\zeta_b}(\boldsymbol{F}_i^S + \boldsymbol{F}_i^B) \tag{7}$$

where μ is the electrophoretic mobility of the chain, ζ_b is the bead drag coefficient, $\boldsymbol{F}_i^S$ is the total spring force felt by the bead, and $\boldsymbol{F}_i^B$ is the Brownian force.

We nondimensionalize eq 7 on the basis of the length and time scales of a spring: $\ell_s \equiv (k_B T/H)^{1/2}$ and $\tau_b \equiv \ell_s^2/D_b$, respectively, where H is the Hookean spring constant and D_b is the bead diffusivity. The nondimensional variables for the local problem are

$$\hat{\boldsymbol{r}} \equiv \frac{\boldsymbol{r}}{\ell_s},\ \hat{t} \equiv \frac{t}{\tau_b},\ \hat{\boldsymbol{E}} \equiv \frac{\boldsymbol{E}}{E_0},\ \hat{\boldsymbol{F}} \equiv \frac{\boldsymbol{F}}{k_B T/\ell_s} \tag{8}$$

(for the post problem we nondimensionalize $\boldsymbol{E}$ using E_∞). This gives the dimensionless form of the equation of motion

$$\frac{d\hat{\boldsymbol{r}}_i}{d\hat{t}} = Pe_{b,0}\hat{\boldsymbol{E}}(\hat{\boldsymbol{r}}_i) + \hat{\boldsymbol{F}}_i^S + \hat{\boldsymbol{F}}_i^B \tag{9}$$

where $Pe_{b,0} = \mu E_0 \ell_s / D_b$ is the bead Péclet number (or for the post problem, $Pe_{b,\infty} = \mu E_\infty \ell_s / D_b$).

The nondimensional Brownian force is given by

$$\hat{\boldsymbol{F}}_i^B = \sqrt{\frac{24}{\Delta\hat{t}}}[\mathbf{r}_n]_i \tag{10}$$

where $\Delta\hat{t}$ is the dimensionless time step and $[\mathbf{r}_n]_i$ are uniform random numbers such that each component $[\mathbf{r}_n]_i^j \in [-1/2, 1/2]$, where j denotes the coordinate x, y, or z. Equation 10 has been normalized so that it provides the proper variance for the Brownian force to satisfy the fluctuation dissipation theorem.

The net dimensionless spring force on the ith bead is

$$\hat{\boldsymbol{F}}_i^S = \begin{cases} \hat{\boldsymbol{f}}_{i,2}^s & i = 1 \\ \hat{\boldsymbol{f}}_{i,i+1}^s + \hat{\boldsymbol{f}}_{i,i-1}^s & 1 < i < N_b \\ \hat{\boldsymbol{f}}_{i,N_b-1}^s & i = N_b \end{cases} \tag{11}$$

where $\hat{\boldsymbol{f}}_{i,j}^s$ is the force exerted on the ith bead by the jth bead. We have included two contributions to the spring force $\hat{\boldsymbol{f}}_{i,j}^s = \hat{\boldsymbol{f}}_{i,j}^{s,b} + \hat{\boldsymbol{f}}_{i,j}^{s,w}$. The first is the simple bulk Hookean spring force

$$\hat{\boldsymbol{f}}_{i,j}^{s,b} = \hat{\mathbf{r}}_j - \hat{\mathbf{r}}_i \tag{12}$$

The second contribution $\hat{\boldsymbol{f}}_{i,j}^{s,w}$ is a correction for the presence of the post/wall.

When a spring is located near an impenetrable surface, it disrupts the underlying random walk upon which the entropic spring force is based. In bulk, the configuration space of a Gaussian chain exhibits axial symmetry around its spring (end-to-end) vector. This leads to a Hookean spring force that is always directed along the direction of the spring vector as is manifest in eq 12. However, in the presence of a surface, the chain's configuration space is restricted, and this axial symmetry is broken. This leads to purely entropic forces that push the chain away from the surface and that are not necessarily directed along the direction of the spring vector. Consideration of this force renders the spring behavior more realistic and actually allows us to use fewer beads (and, therefore, fewer computational resources) to reach the predicted scaling regimes.

We can account for this effect by including a correction term in the spring force.[32] If the surface is a flat plane that passes through the origin, the correction is given by

$$\hat{\boldsymbol{f}}_{i,j}^{s,w} = \left\{ \frac{2(\hat{\mathbf{r}}_j \cdot \boldsymbol{n}_w)}{\exp[2(\hat{\mathbf{r}}_i \cdot \boldsymbol{n}_w)(\hat{\mathbf{r}}_j \cdot \boldsymbol{n}_w)] - 1} \right\} \boldsymbol{n}_w \tag{13}$$

where $\boldsymbol{n}_w$ is the unit normal pointing out of the surface. This term always pushes the beads away from the wall. It diverges as the beads approach the surface and is sufficient to prevent the beads from passing through the wall, so it has the secondary benefit that we do not have to include an additional force dedicated to imposing the wall excluded volume. This expression can be directly applied for the local problem because the surface is flat. For the post problem, we assume that locally the post looks flat and neglect any correction due to the curvature of the post surface.

The time-stepping scheme we used for the local problem is as follows

$$\Delta\hat{t} = \begin{cases} N_b^{-1} Pe_{b,0}^{-2}/5000 & Pe_{b,0} < N_b^{-3/2} \\ Pe_{b,0}^{-4/3}/5000 & N_b^{-3/2} \le Pe_{b,0} < 1 \\ Pe_{b,0}^{-2}/5000 & Pe_{b,0} \ge 1 \end{cases} \tag{14}$$

For the post problem, we used the same scheme with $Pe_{b,0} = 2Pe_{b,\infty}$.

5. Analysis of Local Problem/Field-Induced Compression

The local problem shown in Figure 1B is characterized by a polymer chain near a flat wall undergoing field-induced

compression by a uniform electrophoretic velocity field, μE_0, applied transverse to the wall in the $-\mathbf{e}_z$ direction. Note that for the local problem we have neglected the curvature inherent in the global post problem. Therefore, we use Cartesian coordinates when describing the local problem, but we will resume using cylindrical coordinates in Section 6 when we return to the global post problem. In our analysis of this problem, we first consider the behavior of a point particle and of a Hookean dumbbell. Using statistical mechanics, we can derive exact analytical results for these cases, which provide basic insight into the problem and a way to validate our numerical model. We then look to blob theory to tackle the more complicated problem of a multibead Gaussian chain.

5.1. Point Particle and Dumbbell. The average distance from the wall for a point particle with a diffusivity of D is easily shown to be $\langle d_w^{pp}\rangle = D/\mu E_0$. This result owes its simplicity to the fact that there is no geometric length scale in the problem because the wall is infinitely large, and the particle is infinitely small. (There is no spring to consider in this case.) Therefore, the only length scale is the dynamic one, $\langle d_w^{pp}\rangle$, which follows from balancing the opposing forces of convection and diffusion on the particle. If we arbitrarily define a field-independent length scale ℓ for the problem, then the result for a point particle becomes

$$\frac{\langle d_w^{pp}\rangle}{\ell} = Pe_\ell^{-1} \tag{15}$$

where $Pe_\ell = \mu E_0 \ell/D$ is a Péclet number based on the arbitrary length scale, ℓ. This result is useful because we expect that even large multibead chains should recover point particle behavior when the applied field strength is extremely weak.

The derivation for the average distance from the wall for a Hookean dumbbell $\langle d_w^{db}\rangle$ is more involved. Because of the linearity of the Hookean spring, all three dimensions act independently, and the problem is 1D in the $\mathbf{e}_z$ direction. The probability density of finding a dumbbell with a center of mass located at d_w and a spring length of q is proportional to the Boltzmann distribution

$$P(d_w, q) \sim \exp\left(-2Pe_{b,0}\frac{d_w}{\ell_s}\right)\left[\exp\left(-\frac{1}{2}\frac{q^2}{\ell_s^2}\right) - \exp\left(-2\frac{d_w^2}{\ell_s^2}\right)\right] \tag{16}$$

where $Pe_{b,0} = \mu E_0 \ell_s/D_b$. From this, we can determine the average distance from the wall

$$\frac{\langle d_w^{db}\rangle}{\ell_s} = \frac{1}{2}\frac{\exp\left(-\frac{1}{2}Pe_{b,0}^2\right)\left(Pe_{b,0}^{-1} + Pe_{b,0}\right) + \sqrt{\frac{\pi}{2}}\operatorname{erfc}\left(\frac{1}{\sqrt{2}}Pe_{b,0}\right)\left(Pe_{b,0}^{-2} - 2 - Pe_{b,0}^2\right)}{\sqrt{\frac{\pi}{2}}\operatorname{erfc}\left(\frac{1}{\sqrt{2}}Pe_{b,0}\right)\left(Pe_{b,0}^{-1} + Pe_{b,0}\right) - \exp\left(-\frac{1}{2}Pe_{b,0}^2\right)} \tag{17}$$

This result is shown in Figure 2.

There are two regimes connected by a transition region that describe the behavior of $\langle d_w^{db}\rangle$. The first is a weak field regime where $Pe_{b,0} \ll 1$. Under these conditions, the dumbbell typically is far away from the wall and only occasionally interacts with it. Therefore, the dumbbell behaves very much like a point particle. Indeed, in the limit of $Pe_{b,0} \ll 1$ the expression given in eq 17 reduces to $\langle d_w^{db}\rangle/\ell_s \approx (2Pe_{b,0})^{-1}$ which is the expected behavior of a point particle with a diffusivity of $D = D_b/2$. (See Figure 2.)

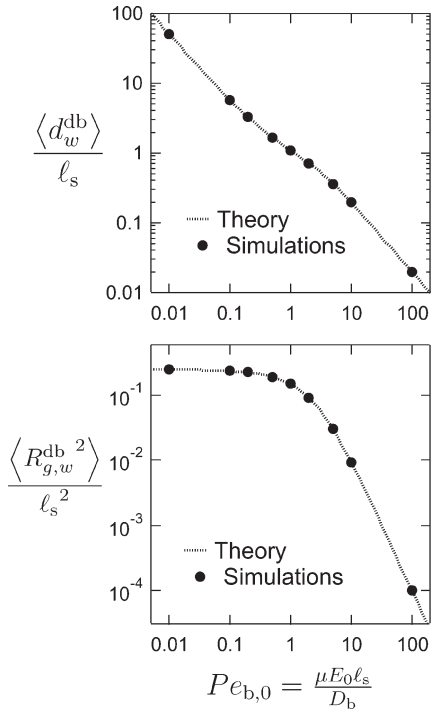

Figure 2. Plot of the average distance of the center of mass $\langle d_w^{db}\rangle$ from a flat wall for a Hookean dumbbell in a uniform field versus the field strength for the BD simulations along with the analytical result given by eq 17 (top). Plot of the radius of gyration squared of a Hookean dumbbell in the direction transverse to the wall $\langle R_{g,w}^{db\ 2}\rangle$ versus the field strength for the simulations and the exact solution given by eq 18 (bottom).

The transition region occurs around $Pe_{b,0} \approx 1$. At this field strength, $\langle d_w^{db}\rangle$ is comparable to the equilibrium spring length ℓ_s, and the dumbbell no longer acts like a single point particle. This can clearly be seen by considering the 1D radius of gyration of the dumbbell in the direction transverse to the wall $R_{g,w}^{db}$, which is given by

$$\frac{\langle R_{g,w}^{db\ 2}\rangle}{\ell_s^2} = \frac{1}{12}\frac{\sqrt{\frac{\pi}{2}}\operatorname{erfc}\left(\frac{1}{\sqrt{2}}Pe_{b,0}\right)Pe_{b,0}\left(3Pe_{b,0}^{-2} + 6 + Pe_{b,0}^2\right) - \exp\left(-\frac{1}{2}Pe_{b,0}^2\right)\left(5 + Pe_{b,0}^2\right)}{\sqrt{\frac{\pi}{2}}\operatorname{erfc}\left(\frac{1}{\sqrt{2}}Pe_{b,0}\right)\left(Pe_{b,0}^{-1} + Pe_{b,0}\right) - \exp\left(-\frac{1}{2}Pe_{b,0}^2\right)} \tag{18}$$

and can also be seen in Figure 2. For $Pe_{b,0} \ll 1$, $\langle R_{g,w}^{db\ 2}\rangle/\ell_s^{\ 2}$ remains unperturbed and maintains a constant value of 1/4. But as $Pe_{b,0}$ approaches 1, $\langle R_{g,w}^{db\ 2}\rangle/\ell_s^{\ 2}$ begins to drop as the internal mode of the dumbbell is affected by the wall presence.

The second regime is a high field limit where $Pe_{b,0} \gg 1$. When the field strength is very large, the dumbbell is strongly pushed against the wall, and both beads are always very near the wall surface ($r_{1,z}/\ell_s, r_{2,z}/\ell_s \ll 1$). This also guarantees that the distance between the beads in the transverse direction is always very small compared to the equilibrium spring size ($|r_{2,z} - r_{1,z}|/\ell_s \ll 1$). The result of these two conditions is that the transverse component of the bulk spring force $(\hat{\boldsymbol{f}}_{i,j}^{s,b})_z$ given by eq 12 is negligible, and the wall correction for the spring force on the ith bead $(\hat{\boldsymbol{f}}_{i,j}^{s,w})_z$ given by eq 13 approaches $\approx (r_{i,z}/\ell)^{-1}$. These two findings indicate that the beads become

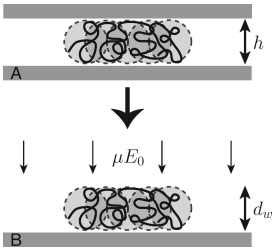

Figure 3. Cartoon depicting the blob scaling approach used to find d_w. The results for slitlike confinement are used to find the entropic penalty for confinement. This energy is then added to an electrical energy in the case of field-induced confinement. The total energy is minimized to find d_w.

uncoupled in the $\mathbf{e}_z$ direction when the dumbbell is pushed strongly against the wall. So for large field strengths, the two ends of the dumbbell should act independently of each other and behave as point particles of diffusivity $D = D_b$. Indeed, in the limit of $Pe_{b,0} \gg 1$, eq 17 reduces to $\langle d_w^{db} \rangle / \ell_s \approx 2 Pe_{b,0}^{-1}$, which, except for the factor of 2, is the expected result for a point particle. (See Figure 2.) The factor of 2 comes from the wall correction for the spring force $(\hat{\boldsymbol{f}}_{i,j}^{s,w})_z \approx (r_{i,z}/\ell)^{-1}$, which does not exist in the case of a true point particle. But this additional force does not change the predicted scaling with $Pe_{b,0}$; it just affects the numerical prefactor.

Also shown in Figure 2 are the results from our BD simulations of a molecule pushed against a flat wall. The data from the simulations match the exact analytical results, thereby validating our numerical model.

5.2. Multibead Chain. The added complexity of multibead chains does not allow for exact analytical solutions; however, on the basis of the point particle and dumbbell results, we can predict the behavior of multibead chains at both very small and very large $Pe_{b,0}$. Additionally, the increased number of internal modes leads to the emergence of a third, intermediate "blob" regime, where globally a chain is strongly deformed by the applied field, but locally individual springs remain virtually unperturbed from their equilibrium configurations.

For very strong field strengths where $Pe_{b,0} \gg 1$, the beads become uncoupled in the transverse direction, just as they do in the case of a dumbbell. Therefore, the individual beads behave very much like point particles so that $\langle d_w \rangle / \ell_s \approx 3 Pe_{b,0}^{-1}$ in the case of $N_b \gg 1$. The prefactor is different from the dumbbell result because, except for the ends, each bead is connected to two springs instead of just one. Additionally, it can be shown that $\langle R_{g,w}^2 \rangle / \ell_s^2 \approx 3 Pe_{b,0}^{-2}$.

For very weak field strengths (we will define how weak momentarily), we expect to recover the point particle behavior exhibited by a dumbbell. In the case of a chain with N_b beads, the chain diffusivity is given by $D = D_b/N_b$ (we assume that the chains are free-draining), and we predict that $\langle d_w \rangle / \ell_s \approx (N_b Pe_{b,0})^{-1}$. Additionally, we expect the 1D radius of gyration to take on its equilibrium value of $\langle R_{g,w}^2 \rangle_{eq} / \ell_s \approx N_b/6$ (which assumes $N_b \gg 1$). The weak field regime is characterized by the condition that $\langle d_w \rangle \gg (\langle R_{g,w}^2 \rangle_{eq})^{1/2}$, which guarantees that the configuration of the chain is nearly unperturbed from its equilibrium configuration. This condition is first violated when $(N_b Pe_{b,0})^{-1} \approx (N_b/6)^{1/2}$. So, we can say that weak field regime is defined for $Pe_{b,0} \ll N_b^{-3/2}$.

This leaves a large region between the weak and high field regimes where $N_b^{-3/2} \ll Pe_{b,0} \ll 1$. This is the new "blob" regime that emerges as N_b increases, and it is characterized by strong global deformation of the chain structure while leaving smaller subunits of the chain fairly unperturbed. These subunits are referred to as "blobs" and are often used in scaling analyses associated with chains confined in slits and tubes. We can make use of the blob theory framework to analyze the problem of field-induced confinement by introducing an electrical energy associated with the applied electrophoretic velocity field as shown in Figure 3.

We start by considering the well-known problem of a chain confined between two parallel plates separated by a distance h. For an ideal chain consisting of N_K Kuhn steps of length b_K, it can be shown that the energy required to confine the chain is proportional to the number of blobs formed[33] and scales as

$$G_{conf} \approx k_B T N_K \left(\frac{h}{b_K} \right)^{-2} \tag{19}$$

In the case of field-induced confinement, we replace the constant plate separation, h, with a field-dependent compression size, d_w. (See Figure 3.) We also introduce an electrical energy for the chain

$$G_{elec} \approx N_K q_{K,eff} E_0 d_w \tag{20}$$

where $q_{K,eff}$ is the effective charge of a Kuhn segment. $q_{K,eff}$ can be derived by considering the free solution electrophoresis of a Kuhn segment. By balancing the electric force, $q_{K,eff}E_0$, driving the segment forward against the opposing drag force $-\zeta_K \nu = -\zeta_K \mu E_0$, where ζ_K is the drag coefficient for a Kuhn step, we discover that $q_{K,eff} = \zeta_K \mu$.

By minimizing the total energy $G_{tot} \approx G_{conf} + G_{elec}$ with respect to d_w, we find that

$$\frac{\langle d_w \rangle}{b_K} \approx \left(\frac{b_K \mu E_0}{k_B T / \zeta_K} \right)^{-1/3} \approx Pe_K^{-1/3} \tag{21}$$

where Pe_K is a Péclet number based on a Kuhn step. It is interesting to note that d_w is independent of chain length in the blob regime. This is because adding chain length increases the number of blobs, but it does not change their size.

Also, we expect in the blob and high-field regimes that $R_{g,w} \approx d_w$. This is reasonable because both describe the size of the compressed chain given that it is always pushed against the wall. This is not the case in the weak field regime, where $R_{g,w}$ is basically unperturbed from its bulk value.

Finally, we can adapt these results to bead−spring chains by substituting springs for Kuhn steps. In doing so, we replace b_K with ℓ_s, ζ_K with ζ_b, and Pe_K with $Pe_{b,0}$.

Combining all of our above predictions for multibead chains, we have for the average distance from the wall

$$\frac{\langle d_w \rangle}{\ell_s} \approx \begin{cases} (N_b Pe_{b,0})^{-1} & Pe_{b,0} \ll N_b^{-3/2} \\ \alpha Pe_{b,0}^{-1/3} & N_b^{-3/2} \ll Pe_{b,0} \ll 1 \\ 3 Pe_{b,0}^{-1} & Pe_{b,0} \gg 1 \end{cases} \tag{22}$$

and for the average 1D radius of gyration squared

$$\frac{\langle R_{g,w}^2 \rangle}{\ell_s^2} \approx \begin{cases} N_b/6 & Pe_{b,0} \ll N_b^{-3/2} \\ \beta Pe_{b,0}^{-2/3} & N_b^{-3/2} \ll Pe_{b,0} \ll 1 \\ 3 Pe_{b,0}^{-2} & Pe_{b,0} \gg 1 \end{cases} \tag{23}$$

In both of these expressions, we have included proportionality constants, α and β, to describe the blob regime. This is to highlight the fact that unlike the weak and strong field regimes, we only have scalings for the behavior of the chains

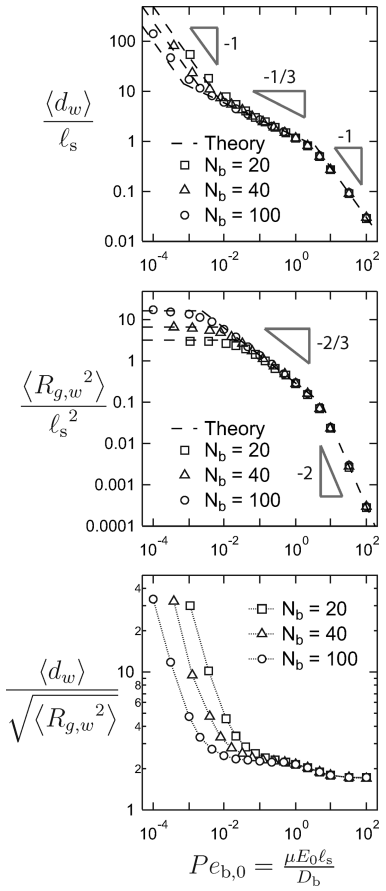

Figure 4. Plot of the average distance of the center of mass from a flat wall $\langle d_w \rangle$ for multibead chains in a uniform field versus the field strength along with the theoretical prediction given by eq 22 (top). Plot of the radius of gyration squared of the chains in the direction transverse to the wall $\langle R_{g,w}{}^2 \rangle$ versus the field strength along with the theoretical prediction given by eq 23 (middle). Plot of the ratio of $\langle d_w \rangle$ and $(\langle R_{g,w}{}^2 \rangle)^{1/2}$ versus the field strength (bottom).

in the blob regime. We have no way of determining α and β a priori, so we must fit real data if we wish to determine them.

To test our predictions, we simulated several different chain lengths (N_b = 20, 40, and 100) at various values of $Pe_{b,0}$. The results of these simulations are shown in Figure 4. The theoretical predictions for the three different regimes given in eqs 22 and 23 are also included as well as slope lines for the predicted scalings.

There is excellent agreement between simulations and theory. The strong and weak field regimes not only exhibit the predicted scalings but also asymptotically approach the predicted quantitative values. The locations of the transitions between regimes are also correctly predicted.

The emergence of an apparent scaling regime with increasing N_b between the strong and weak field regions confirms the existence of a blob regime. Indeed, the simulation results match the predicted blob theory scalings. But to more rigorously demonstrate the existence of the blob regime, we plotted the ratio of $\langle d_w \rangle$ and $(\langle R_{g,w}{}^2 \rangle)^{1/2}$. In regions where both of these quantities are predicted to scale the same way, we expect to see a broad plateau in the plot of their ratio. $\langle R_{g,w}{}^2 \rangle$ is a constant in the weak field regime, so the ratio should diverge as $Pe_{b,0}$ decreases. In the strong field regime, the ratio should plateau to a constant value of $\sqrt{3}$. If the blob regime does indeed exist, then a similar plateau should be seen for $N_{b,0}{}^{-3/2} \ll Pe_{b,0} \ll 1$, although it ought to have a different numerical value than $\sqrt{3}$. This is exactly what is seen in Figure 4, and it clearly and convincingly demonstrates the presence of the predicted blob regime.

It was found that $\alpha = 1.26$ and $\beta = 0.30$ by fitting the results of $N_b = 100$ to the predicted scalings for $\langle d_w \rangle$ and $(\langle R_{g,w}{}^2 \rangle)^{1/2}$, respectively, in the blob regime.

6. Analysis of Global/Post Problem

With our results for the local problem in hand, we are now equipped to address fully the post problem shown in Figure 1A. We begin by determining the average tangential velocity of the molecule, $\langle v_\theta \rangle$. We then use this result to develop a 1D Fokker−Planck equation to balance the effects of convection and diffusion along the post surface. From this, we calculate the mean escape time, $\langle T_{esc} \rangle$, of a molecule as a function of its initial collision location, θ_0. We compare all of our predictions against simulation results.

We also restrict our analysis to field strengths where the compressed chains are in the blob regime for the local problem. Clearly, depending on the strength of the applied field, we could develop different velocity predictions for each of the low-field, high-field, and blob regimes. However, it seems sufficient to analyze only one of these, knowing that the same type of analysis should be applicable to the other two. We have chosen the blob regime because it seems to be the richest of the three.

6.1. Determination of $\langle v_\theta \rangle$. We have previously shown in eq 6 that $\langle v_\theta \rangle \sim \langle d_p \rangle$. From the result in eq 22 for the blob regime, we expect that

$$\langle d_p \rangle \approx \alpha \ell_s Pe_b[\mu E_r(\theta)]^{-1/3} \tag{24}$$

where $Pe_b[\mu E_r(\theta)]$ is the Péclet number based on the local value of $\mu E_r(\theta)$, which is given in eq 5. Combining these results, we arrive at

$$\frac{\langle d_p \rangle}{\ell_s} \approx \alpha(2Pe_{b,\infty} \cos\theta)^{-1/3} \tag{25}$$

If we insert this expression into eq 6, then we find that

$$\frac{\langle v_\theta \rangle}{D_b/N_b R} \approx \alpha N_b (2Pe_{b,\infty})^{2/3} \cos^{-1/3}\theta \sin\theta \tag{26}$$

where we have nondimensionalzed the velocity based on the post length scale, R, and the chain diffusion time scale, $N_b R^2/D_b$. On the basis of this equation for the velocity, we can define a governing Péclet number for the post problem

$$Pe_P = N_b (2Pe_{b,\infty})^{2/3} \tag{27}$$

In Figure 5, we compare the prediction for $\langle d_p \rangle$ versus $Pe_b(\theta)$ given in eq 24 to the results from simulating the collisions of several different chain lengths at various values of Pe_P with a post of radius $R/\ell_s = 50$. Excellent agreement is seen, except for $Pe_P = 40$. This discrepancy at high Pe_P occurs because the smaller chain lengths (N_b = 10 and 20) have been pushed beyond the blob regime into the high field regime ($Pe_b \gg 1$), where eq 24 is not applicable. These results confirm that our analysis of the local problem, particularly eq 22, is correct, even for the more complicated post problem. We also compare our predictions for $\langle v_\theta \rangle$ given in eq 26 to the simulation data in Figure 6. We have nondimensionalized $\langle v_\theta \rangle$ by the predicted scaling $\alpha Pe_P D_b/N_b R$ to achieve universal collapse of all the curves. Our theoretical treatment matches the data, except when blob theory breaks down for the smaller chains at large Pe_P.

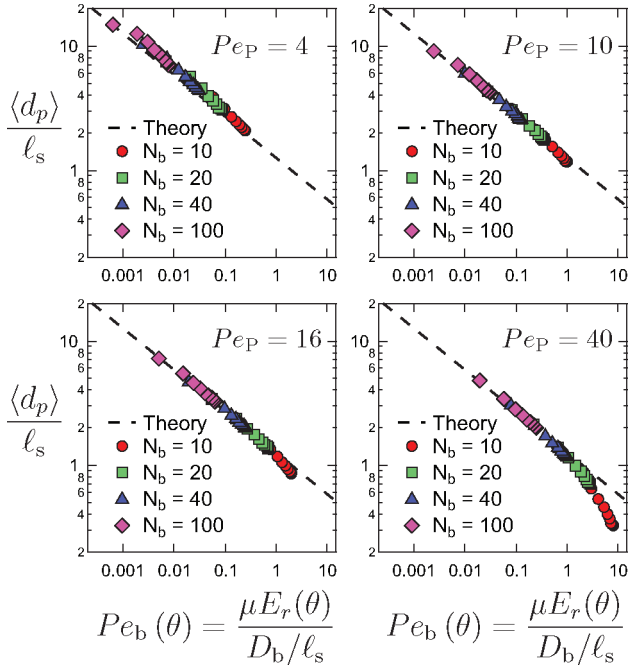

Figure 5. Plot of the average distance of the center of mass from the post surface, $\langle d_p \rangle$, for multibead chains trapped against a conducting post versus the local transverse field strength, μE_r. The fitted scaling from the flat wall studies is shown for comparison (eq 24).

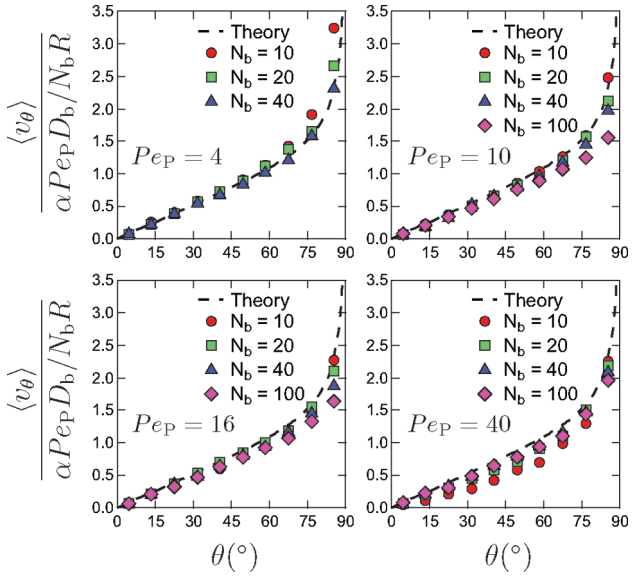

Figure 6. Plots of the average tangential velocity, $\langle v_\theta \rangle$, of multibead chains trapped against a conducting post as a function of location on the post surface, θ. The theoretical prediction given by eq 26 is also plotted.

The velocity $\langle v_\theta \rangle$ at the most upstream point on the post ($\theta = 0$) is zero, and initially, it increases nearly linearly with increasing θ, but $\langle v_\theta \rangle$ begins to rise rapidly as θ approaches $\pi/2$. This is due to a sharp decrease in $\mu E_r(\theta)$ near $\theta = \pi/2$, which causes the chain to expand quickly. This increase in $\langle d_p \rangle$ leads to greater exposure of the chain to the tangential electrophoretic velocity field and a rapid increase in the average molecular velocity, $\langle v_\theta \rangle$. Our prediction for $\langle v_\theta \rangle$ given in eq 26 actually diverges at $\theta = \pi/2$, which is clearly aphysical. This is because our model neglects several realities including that our linearization of μE_θ is not valid for large $\langle d_p \rangle$ and that the chain cannot expand instantaneously (i.e., separation of the radial and angular dynamics breaks down). However, our prediction is still very good over the entire domain, except very near $\theta = \pi/2$.

Another problem with our model is that it predicts that a chain located at $\theta = 0$ will never escape from the post because $\langle v_\theta \rangle = 0$. To predict accurately the behavior of a chain near $\theta = 0$, we must incorporate diffusion into our model.

6.2. Incorporating Diffusion. To include diffusion in our theory, we turn to a Fokker–Planck (FP) approach. We consider the post problem to be a time-dependent 1D problem in the $\mathbf{e}_\theta$ direction with $r = R$. We develop a Fokker–Planck equation for a molecule with a diffusivity of $D = D_b/N_b$. If we assume the molecule is being transported in a velocity field $\langle v_\theta \rangle$, then we can write

$$\frac{\partial p}{\partial t} = \frac{D_b}{N_b}\frac{\partial^2 p}{\partial (R\theta)^2} - \frac{\partial}{\partial (R\theta)}(\langle v_\theta \rangle p) \tag{28}$$

where p is the probability density of finding a molecule at a given time and location and $R\theta$ is the arc length. Because of the symmetry around the most upstream point of the post at $\theta = 0$, we restrict our analysis to the domain $0 \le \theta \le \pi/2$. We use our previously determined expression for $\langle v_\theta \rangle$ given in eq 26. For tractability, we make the approximation $\cos^{-1/3}\theta \sin\theta \approx \theta$, which is very good over most of the domain. Finally, we nondimensionalize time based on the diffusion time scale of the chain over the length scale of the post: $\tau = N_b R^2/D_b$. This leads to the nondimensional form of the FP equation

$$\frac{\partial p}{\partial \tau} = \frac{\partial^2 p}{\partial \theta^2} - \alpha Pe_P \frac{\partial}{\partial \theta}(\theta p) \tag{29}$$

We use a reflecting boundary condition at $\theta = 0$ because of symmetry and an absorbing boundary condition at $\theta = \pi/2$ to signify the "escape" of the molecule

$$\frac{\partial p}{\partial \theta}(\tau, \theta = 0) = p(\tau, \theta = \pi/2) = 0 \tag{30}$$

For the initial condition, we choose a unit impulse at θ_0 to model the initial collision location of a molecule at that location

$$p(\tau = 0, \theta) = \delta(\theta - \theta_0) \tag{31}$$

This is the problem of a particle diffusing in an inverted harmonic potential, and interestingly, it has been considered before in DNA collisions with point obstacles.[17,21] Although we cannot obtain a solution for $p(\tau,\theta)$, we can calculate the mean first passage time to $\theta = \pi/2$ of a particle that starts at $\theta = \theta_0$. This is exactly the average escape time of a molecule from the post surface, $\langle T_{esc} \rangle$. The theory of first passage times[34] tells us that for this particular problem

$$\frac{\langle T_{esc} \rangle}{N_b R^2/D_b} = \int_{\theta_0}^{\pi/2} dx \exp\left(-\frac{\alpha Pe_P}{2} y^2\right) \int_0^x dy \exp\left(\frac{\alpha Pe_P}{2} x^2\right) \tag{32}$$

We can recast this expression in terms of Dawson's integral[35]

$$[D(x) = e^{-x^2} \int_0^x e^{y^2} dy]$$

$$\frac{\langle T_{esc} \rangle}{N_b R^2/D_b} = \sqrt{\frac{2}{\alpha Pe_P}} \int_{\theta_0}^{\pi/2} D\left(\sqrt{\frac{\alpha Pe_P}{2}} x\right) dx \tag{33}$$

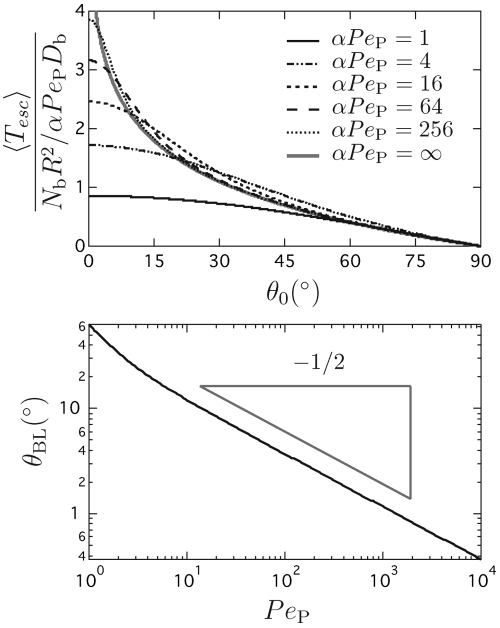

Figure 7. Plots of the average "escape" time $\langle T_{esc}\rangle$ predicted by eq 34 for various values of αPe_P, including the purely convective case (i.e., $Pe_P = \infty$) (top). Plot of the location of the intersection point θ_{BL} of $\langle T_{esc}\rangle$ for a given value of Pe_P with the purely convective case (bottom). The predicted scaling for θ_{BL}, which is a measure of the boundary layer size, is shown for comparison.

Finally, the integral of $D(x)$ can be written in terms of generalized hypergeometric functions[35] $[{}_pF_q(a_1, ..., a_p; b_1, ..., b_q; z)]$

$$\frac{\langle T_{esc}\rangle}{N_b R^2/D_b} = \frac{1}{2}\left[\frac{\pi^2}{4}\,{}_2F_2\left(1,1;3/2,2;-\frac{\alpha Pe_P}{2}\frac{\pi^2}{4}\right) - \theta_0^2\,{}_2F_2\left(1,1;3/2,2;-\frac{\alpha Pe_P}{2}\theta_0^2\right)\right] \quad (34)$$

In Figure 7, we have plotted this prediction for $\langle T_{esc}\rangle$, nondimensionalized by the convective time scale $N_b R^2/\alpha Pe_P D_b$ for several values of Pe_P including for the purely convective case (i.e., $Pe_P = \infty$).

We expect that in the region of the domain dominated by convection the curve will collapse onto the result for pure convection, and indeed, this is what occurs for θ near $\pi/2$, where the velocity is the strongest. Near $\theta = 0$, diffusion dominates, and the curve falls well below that of pure convection because diffusion is helping to speed up the escape process. It is also clear in Figure 7 that the location of this transition from the diffusive region to the convective region occurs at smaller and smaller values of θ as Pe_P increases. This is expected because a larger portion of the domain is dominated by convection at large values of Pe_P. Indeed, this increasingly small diffusive region near $\theta = 0$ forms a boundary layer for $Pe_P \gg 1$.

We can derive a scaling for the size of the region dominated by diffusion θ_{BL} by estimating where the convective and diffusive time scales are comparable. The convective time scale is $N_b R^2/\alpha Pe_P D_b$, whereas the diffusive time scale is $N_b(R\theta_{BL})^2/D_b$. Balancing these two gives the scaling $\theta_{BL} \sim Pe_P^{-1/2}$.

To confirm this scaling for θ_{BL}, we used the location of the intersection of $\langle T_{esc}\rangle$ for a finite Pe_P with the curve for the purely convective case as a measure of θ_{BL}. Figure 7 shows the results of this analysis. At high Pe_P, the predicted scaling is correct.

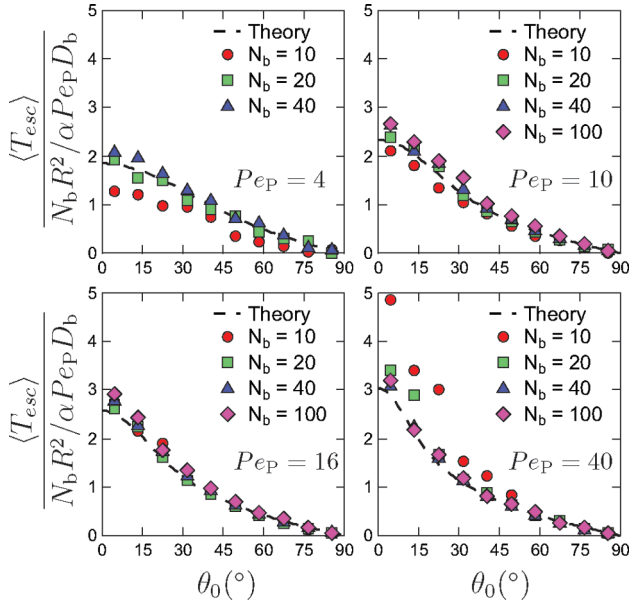

Figure 8. Plots of the average escape time, $\langle T_{esc}\rangle$, of multibead chains as a function of where they are initially trapped by a conducting post, θ_0. The theoretical prediction given by eq 34 is also shown.

The results for $\langle T_{esc}\rangle$ from our simulations are shown in Figure 8, where we have nondimensionalized the escape time by the convective time scale. Good agreement is seen between the simulations and the predictions of eq 34. The only notable exception is for $N_b = 10$ at $Pe_P = 40$, which is expected because the chain has been pushed well beyond the blob regime, as previously shown. Our model clearly does a very good job of predicting the behavior of these chains.

7. Conclusions

We have examined the problem of electrophoretic collisions of DNA with large, ideally conducting posts, and we have identified and characterized the essential physics that govern the problem. We have purposefully simplified this problem to develop analytically solvable models and scaling theories that prove that the important physics are well understood. In particular, we have studied the field-induced compression a molecule against the post surface and how it determines the velocity of the chain as it moves around the post. Although we have used the simple model of an ideal, Gaussian chain, we believe the basic physics and fundamental character of the problem have been captured. However, our approach allows for a more realistic molecular description. For example, excluded volume effects could easily be incorporated into our blob theory framework, and new scalings could be derived.

Also, by considering large posts, we have precluded all hooking phenomena, but in applications involving DNA separations, hooking and the subsequent unhooking process are typically the major reasons that length-dependent separation arises. However, our results can still be applied to examine the more realistic and complicated situation of moderately sized conducting posts where hooking should occur. For example, our prediction for the tangential velocity of a molecule (eq 26) is nearly linear in θ, which makes it look very similar to an elongational field. This suggests that for strong enough field gradients, molecules will stretch around the post. Such behavior would be important for understanding hook formation in these more realistic cases.

We believe that conducting posts could offer advantages over insulating posts because of the way they attract and directly

interact with DNA molecules. Insulating and dielectrically matched posts tend to move molecules around their surfaces quickly, and detrimental channeling is often seen in arrays of such posts.[31] The attractive nature of conducting posts might decrease the effects of channeling and enhance separation efficiency. Additionally, it could also lead to new modes of separation that have not yet been observed or predicted.

Currently, we know of no experimental studies that have looked at conducting posts, but we can imagine at least two different ways to achieve such a system. The first would be to use metal posts with biased AC fields. Because metal posts are impenetrable to ions, a DC field would simply polarize the surrounding double layer, and eventually, the field lines would resemble those of an insulating post. Using properly timed AC fields should prevent this polarization from occurring.[36] The second way would be to use a charged hydrogel that is impermeable to DNA. Unlike a metal post, a charged hydrogel would be permeable to small ions, and its higher conductivity than the bulk fluid would result in the desired field lines.

To end, we would like to provide estimates of some of the parameters and measurables that might be used or seen in a real experiment under reasonable conditions. For order of magnitude purposes, we assume that for DNA in buffers typically used by our group[22] and others, the length and the diffusivity of a Kuhn segment are around $b_K \approx 100$ nm and $D_K \approx 20\ \mu m^2/s$, respectively, and that a typical value for the electrophoretic mobility is $\mu \approx 1.5\ \mu m/s$. For T4-DNA, which has a contour length of $L \approx 70\ \mu m$, a bulk radius of gyration of $R_g \approx 1.5\ \mu m$, and a bulk diffusivity of $D \approx 1\ \mu m^2/s$, we estimate that the blob regime occurs at applied field strengths in the range of $E_\infty \approx 0.005-50$ V/cm. We obtain this estimate from eq 22 by replacing the bead Péclet number, Pe_b, with the Péclet number based on a Kuhn step, Pe_K. Using this range of field strengths, we can estimate the characteristic escape time, T_{esc}, for a particular post size using the convective time scale of the global post problem, $R^2/(2Pe_{K,\infty})^{2/3}D_K$. However, we must also ensure that the convective time scale is faster than the diffusive time scale, R^2/D, which provides the upper limit for T_{esc}. On the basis of this calculation, we find that the convection-dominated blob regime occurs in the range of $E_\infty \approx 1-50$ V/cm. For a post size of $R = 5\ \mu m$, the characteristic escape time would be $T_{esc} \approx 1-20$ s. For a post size of $R = 15\ \mu m$, this would increase to $T_{esc} \approx 10$ s to 3 min.

Acknowledgment. We thank the Singapore-MIT Alliance for Research and Technology (SMART) and the National Science Foundation grant CBET-0852235 for funding. Additionally, we would like to thank Jing Tang and Will Uspal for their many insightful discussions.

References and Notes

(1) Perkins, T.; Smith, D.; Chu, S. *Science* **1997**, *276*, 2016.
(2) Bakajin, O.; Duke, T.; Chou, C.; Chan, S.; Austin, R.; Cox, E. *Phys. Rev. Lett.* **1998**, *80*, 2737.
(3) Turner, S.; Cabodi, M.; Craighead, H. *Phys. Rev. Lett.* **2002**, *88*, 128103.
(4) Schroeder, C.; Babcock, H.; Shaqfeh, E.; Chu, S. *Science* **2003**, *301*, 1515.
(5) Balducci, A.; Hsieh, C.; Doyle, P. *Phys. Rev. Lett.* **2007**, *99*, 238102.
(6) Bonthuis, D. J.; Meyer, C.; Stein, D.; Dekker, C. *Phys. Rev. Lett.* **2008**, *101*, 108303.
(7) Doyle, P.; Bibette, J.; Bancaud, A.; Viovy, J. *Science* **2002**, *295*, 2237.
(8) Han, J.; Craighead, H. *Science* **2000**, *288*, 1026.
(9) Kaji, N.; Tezuka, Y.; Takamura, Y.; Ueda, M.; Nishimoto, T.; Nakanishi, H.; Horiike, Y.; Baba, Y. *Anal. Chem.* **2004**, *76*, 15.
(10) Chan, E.; Goncalves, N.; Haeusler, R.; Hatch, A.; Larson, J.; Maletta, A.; Yantz, G.; Carstea, E.; Fuchs, M.; Wong, G.; Gullans, S.; Gilmanshin, R. *Genome Res.* **2004**, *14*, 1137.
(11) Jo, K.; Dhingra, D.; Odijk, T.; de Pablo, J.; Graham, M.; Runnheim, R.; Forrest, D.; Schwartz, D. *Proc. Natl. Acad. Sci. U.S.A.* **2007**, *104*, 2673.
(12) Sevick, E. M.; Williams, D. R. M. *Phys. Rev. E* **1994**, *50*, R3357.
(13) Nixon, G.; Slater, G. *Phys. Rev. E* **1994**, *50*, 5033.
(14) Saville, P.; Sevick, E. *Macromolecules* **1999**, *32*, 892.
(15) Randall, G.; Doyle, P. *Phys. Rev. Lett.* **2004**, *93*, 058102.
(16) Kim, J. M.; Doyle, P. S. *Macromolecules* **2007**, *40*, 9151.
(17) Laachi, N.; Cho, J.; Dorfman, K. D. *Phys. Rev. E* **2009**, *79*, 031928.
(18) Dorfman, K. D., under review.
(19) Duke, T.; Austin, R.; Cox, E.; Chan, S. *Electrophoresis* **1996**, *17*, 1075.
(20) Minc, N.; Futterer, C.; Dorfman, K.; Bancaud, A.; Gosse, C.; Goubault, C.; Viovy, J. *Anal. Chem.* **2004**, *76*, 3770.
(21) Volkmuth, W. D.; Duke, T.; Wu, M. C.; Austin, R. H.; Szabo, A. *Phys. Rev. Lett.* **1994**, *72*, 2117.
(22) Randall, G. C.; Doyle, P. S. *Macromolecules* **2006**, *39*, 7734.
(23) Teclemariam, N. P.; Beck, V. A.; Shaqfeh, E. S. G.; Muller, S. J. *Macromolecules* **2007**, *40*, 3848.
(24) Dorfman, K. D. *Phys. Rev. E* **2006**, *73*, 061922.
(25) Balducci, A.; Doyle, P. S. *Macromolecules* **2008**, *41*, 5485.
(26) de Gennes, P. *Science* **1997**, *276*, 1999.
(27) Randall, G.; Doyle, P. *Macromolecules* **2005**, *38*, 2410.
(28) André, P.; Long, D.; Ajdari, A. *Eur. Phys. J. B* **1998**, *4*, 307.
(29) Patel, P.; Shaqfeh, E. *J. Chem. Phys.* **2003**, *118*, 2941.
(30) Mohan, A.; Doyle, P. S. *Phys. Rev. E* **2007**, *76*, 040903.
(31) Ou, J.; Cho, J.; Olson, D. W.; Dorfman, K. D. *Phys. Rev. E* **2009**, *79*, 061904.
(32) Woo, N.; Shaqfeh, E.; Khomami, B. *J. Rheol.* **2004**, *48*, 281.
(33) Rubinstein, M.; Colby, R. H. *Polymer Physics*; Oxford University Press: New York, 2003.
(34) Gardiner, C. W. *Handbook of Stochastic Methods for Physics, Chemistry, and the Natural Sciences*; Springer: New York, 1983.
(35) Abramowitz, M.; Stegun, I. A. *Handbook of Mathematical Functions*; Dover Publications: New York, 1964.
(36) Squires, T. M.; Bazant, M. Z. *J. Fluid Mech.* **2004**, *509*, 217.